Journal of Alloys and Compounds 554 (2013) 97–103

Contents lists available at SciVerse ScienceDirect

Journal of Alloys and Compounds

journal homepage: www.elsevier.com/locate/jalcom

Room temperature structure and multiferroic properties in $Bi_{0.7}La_{0.3}FeO_3$ ceramics

T.T. Carvalho [a,*], J.R.A. Fernandes [b,c], J. Perez de la Cruz [b], J.V. Vidal [d], N.A. Sobolev [d], F. Figueiras [e], S. Das [e], V.S. Amaral [e], A. Almeida [f], J. Agostinho Moreira [f], P.B. Tavares [a]

[a] CQVR and Chemistry Department, University of Trás-os-Montes and Alto Douro, Apartado 1013, 5001-801 Vila Real, Portugal
[b] INESC TEC, Optoelectronic and Electronic System Unit, Rua do Campo Alegre, 687, 4169-007 Porto, Portugal
[c] Physics Department, University of Trás-os-Montes and Alto Douro, Apartado 1013, 5001-801 Vila Real, Portugal
[d] Physics Department and I3N, University of Aveiro, 3810-193 Aveiro, Portugal
[e] Physics Department and CICECO, University of Aveiro, 3810-193 Aveiro, Portugal
[f] IFIMUP and IN-Institute of Nanoscience and Nanotechnology, Faculty of Sciences, University of Porto, Rua do Campo Alegre, 687, 4169-007 Porto, Portugal

ARTICLE INFO

Article history:
Received 12 July 2012
Received in revised form 31 October 2012
Accepted 2 November 2012
Available online 17 November 2012

Keywords:
Ceramics
Multiferroic materials
Magnetoelectric
$BiFeO_3$

ABSTRACT

Single phase $Bi_{0.7}La_{0.3}FeO_3$ ceramic samples were successfully synthesized by sol–gel combustion and co-precipitation methods, performing a final sintering at 820–870 °C from 10 up to 180 min. Rietveld refinements of the XRD data detected small satellite peaks that were successfully indexed by an incommensurated modulated structure model. Lanthanum doping improves magnetic response, reduces the leakage current and dielectric losses. The piezoelectric coefficient was reported for the first time in the $Bi_{0.7}La_{0.3}FeO_3$ composition.

1. Introduction

Bismuth ferrite, $BiFeO_3$ (BFO) is one of the most promising multiferroic materials due to its high Curie (1000 K) and Néel temperatures (643 K) [1]. Several applications are foreseen including memories, telecommunication and security applications, photovoltaic devices and catalyzed water treatments [2–4]. Moreover, most of the applied research is related to magnetoelectric and spintronics such as memories that can be written using electric field and read using a magnetic field. Nevertheless, the widespread use of this material in industrial applications depends on solving several problems such as the formation of secondary phases, the high dielectric losses, high leakage currents and high coercive electric fields at room temperature [5].

Various attempts have been made to reduce leakage currents in films including the use of single crystal substrates [6], buffer layers [7], heterostructures [8] or by replacing the Bi or the Fe ions [9,10].

The replacement of a small amount of metal helps to stabilize the $BiFeO_3$ phase. For $Bi_{1-x}A_xFeO_3$, the most studied elements as potential substituents for the A position are in the lanthanide series (La, Pr, Nd, Sm, Eu, Gd, Tb, Dy and Yb) [9,11]. Lanthanum is the most investigated rare earth substitute in A position. Numerous investigations have been undertaken in this system. However, a large controversy persists regarding the effects in physical properties by isovalent substitution of bismuth ions (Bi^{3+}) for rare earth ions like La^{3+} ($Bi_{1-x}La_xFeO_3$). It is generally accepted that La inhibits the formation of secondary phases [12] and decreases leakage currents [13]. While for the ferroelectric coercive field an ambiguous behavior is reported, some authors observed that the La doping can increase the coercive field [14], however Simões and his coworkers reported a decrease in coercive field for 15% lanthanum concentration [13].

One of the most controversial aspects of $Bi_{1-x}La_xFeO_3$ is their structural phase diagram at room temperature. It is generally accepted that for $x < 0.15$, the system crystallizes in a non centrosymmetric *R3c* polar structure [1]. However for $x > 0.15$ five different crystallographic phases are proposed, *P1*, *C222*, $C222_1$, $Pn2_1a$ and *Pnma* with boundaries at 0.24, 0.40, 0.55 and 0.7 respectively [15,16]. Moreover, recent report suggests an antipolar *Pbam* structure for $0.18 < x < 0.43$ [17]. Studies suggesting that two phases (rhombohedral and orthorhombic phases) can coexist are frequently found [18]. Even for the compositions with $x = 0.25$ and $x = 0.30$, different orthorhombic structures have been proposed: the centrosymmetric *Pnma* or *Imma* [16,18] or the non centrosymmetric $Pn2_1a$ or *C222* [23]. A recent investigation by Rusakov et al. using electron diffraction, HR-TEM and synchrotron XRD at room temperature, revealed an incommensurately modulated phase with $Imma(00\gamma)s00$ superspace group for $Bi_{0.75}La_{0.25}FeO_3$. [16].

* Corresponding author.
E-mail address: tcarvalho@utad.pt (T.T. Carvalho).

0925-8388/$ - see front matter © 2012 Elsevier B.V. All rights reserved.
http://dx.doi.org/10.1016/j.jallcom.2012.11.018

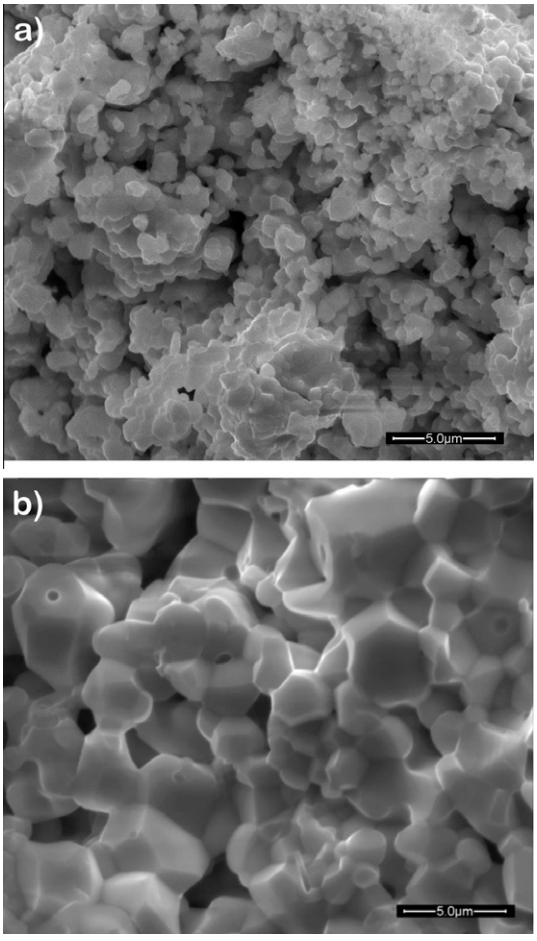

Fig. 1. SEM images showing grain morphology of the $Bi_{0.7}La_{0.3}FeO_3$ samples thermal treated at (a) 820 °C/1 h; (b) 870 °C/3 h.

$Bi_{1-x}La_xFeO_3$ ($0 \leqslant x \leqslant 0.20$) piezoelectric measurements were only reported once by Jiang et al., and the highest piezoelectric coefficient reached was 11.5 pC/N for $x = 0.05$. [12].

Another important effect of La substitution in bismuth ferrite system is the enhancement of magnetic properties. The pure $BiFeO_3$ is a G-type canted antiferromagnetic (AFM) modulated by a 62 nm cycloid spin. While sintered $BiFeO_3$ ceramics show AFM behavior without magnetic hysteresis, such cycles can only be seen in BFO nanoparticles and thin films [19–21]. The La doping promotes the disappearance of the cycloid spin structure therefore it increases remnant magnetization and it leads to magnetic hysteresis loops [22]. In $Bi_{0.7}La_{0.3}FeO_3$ ceramic samples, the magnetic remnant magnetization ranges from 0.027 up to 0.27 emu g^{-1} [23,24].

Different studies point out the magnetic properties of $Bi_{0.7}La_{0.3}FeO_3$ although controversy persists about the structure and ferroelectric properties.

We studied the crystal structure of $Bi_{0.7}La_{0.3}FeO_3$ closely. With the purpose of determining the symmetry of $Bi_{0.7}La_{0.3}FeO_3$, physical macroscopic properties (polarization and magnetization) were analyzed at room temperature.

2. Experimental details

$Bi_{0.7}La_{0.3}FeO_3$ ceramic samples were prepared using the urea sol–gel combustion method, as reported elsewhere [25]. In order to compare results, some samples were also prepared using the co-precipitation method [26]. The resulting powders were calcinated at 550 °C, regrounded, pelletized and thermally treated at 820–870 °C from 10 min up to 3 h, with fast heating and cooling rates (up to 200 °C/min). This process is usually called *rapid thermal annealing* and has been used in order to suppress the Fe^{2+} and oxygen vacancies which are associated with high leakage currents [27,28]. All the measurements were performed in samples sintered at 820 °C for 10 min with the exception of the polarization and piezoelectric measurements where the 840 °C/10 min samples were used due to their higher mechanical resistance. X-ray diffraction measurements and SEM analysis were performed in all samples. The apparent density was calculated using a Vernier Caliper to measure the height and the diameter of the pellet and weighed on a laboratory balance. The real density was calculated from the unit cell parameters after X-ray diffraction data refinement.

Powder X-ray diffraction (XRD) data were collected at room temperature by *PANalytical X'Pert Pro* diffractometer, equipped with *X'Celerator* detector and secondary monochromator in $\theta/2\theta$ Bragg–Bentano geometry. The measurements were carried out using a CuKα radiation ($\lambda_{\alpha 1}$ = 1.54060 Å and $\lambda_{\alpha 2}$ = 1.54443 Å) in a 15–100° 2θ angular range, a step width of 0.017° and a counting time up to 1500 s/step. The patterns were analyzed by Rietveld method with PowderCell® [29], Rietica® [30] and Jana2006® [31] software. The grain morphology and composition were analyzed by SEM/EDS with a *FEI Quanta 400/EDAX*.

The Raman-scattering studies were performed with polished pellets of about $3 \times 4 \times 1$ mm^3 size. The unpolarized Raman spectra have been measured at room temperature under the backscattering geometry, using an *Olympus* microscope BH-2, with an objective of 50×. The 514.5 nm polarized line of an Ar+ laser was used for excitation with an incident power of about 5 mW impinging on the sample in order to avoid heating. The scattered light was analyzed using a *T64000 Jobin–Yvon* spectrometer, operating in a triple subtractive mode, and equipped with a liquid-nitrogen-cooled charged–coupled device. Identical conditions were maintained for all scattering measurements. The spectral slit width was about 1.5 cm^{-1}. The Raman spectra were analyzed by fitting a sum of independent oscillator, according to the general formula:

$$I(\omega, T) = (1 + n(\omega, T))\sum_{j=1}^{N} A_{oj} \frac{\omega \Omega_{oj}^2 \Gamma_{oj}}{(\Omega_{oj}^2 - \omega^2)^2 + \omega^2 \Gamma_{oj}^2} \quad (1)$$

where $n(\omega,T)$ is the Bose–Einstein temperature factor, and A_{oj}, Ω_{oj} and Γ_{oj} are the amplitude, the frequency and the damping factor for the j-th normal mode. The fitting was made with the software package IgorPro (WaveMetrics®).

Sputtered gold electrodes were deposited for 10 min under a 20 mA argon current using a Scancoat Six sputter coater (BOC Edwards) with a golden target.

The leakage current measurements were performed at room temperature using a programmable picoammeter *Keithley 6487* controlled by a LabView® program, samples were pre-poled during 5 min at maximum field, followed by a relaxation step of 10 min.

$P(E)$ was recorded at room temperature, using a modified Sawyer–Tower circuit [32]. In this circuit, the reference capacitor can have values between 47 nF and 1 μF. In order to prevent any masking of the actual domain reversal by some additional dynamic response, the frequency chosen for measurement of the $P(E)$ cycles was 1.3 Hz. However, higher and lower frequencies were also tested without significant changes.

Computer assisted dielectric characterization was performed as a function of temperature, using an Agilent E4980A precision LCR meter. The measurements were obtained at room temperature on a wide frequency interval of 1 kHz–1 MHz.

A fiber optic double beam interferometer system was used for measuring the d_{33} piezoelectric coefficient of the ceramics. The measurements were carried out at 2 kHz. The accuracy of the measurement was checked with a quartz crystal. Details of the interferometric measurements have been reported elsewhere [33].

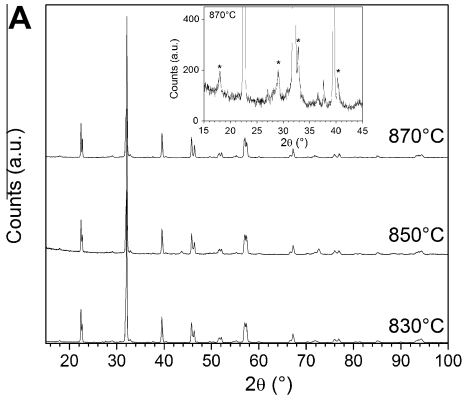

Fig. 2. (A) Diffraction patterns of $Bi_{0.7}La_{0.3}FeO_3$ samples prepared by sol–gel combustion and thermal treated at 830, 850 and 870 °C for 1 h; detail showing small peaks (∗) not predicted by conventional symmetry groups; (B) results of Rietveld refinement with Rietica software: (a) P*nma*; (b) P$n2_1a$; (c) I*mma* structures.

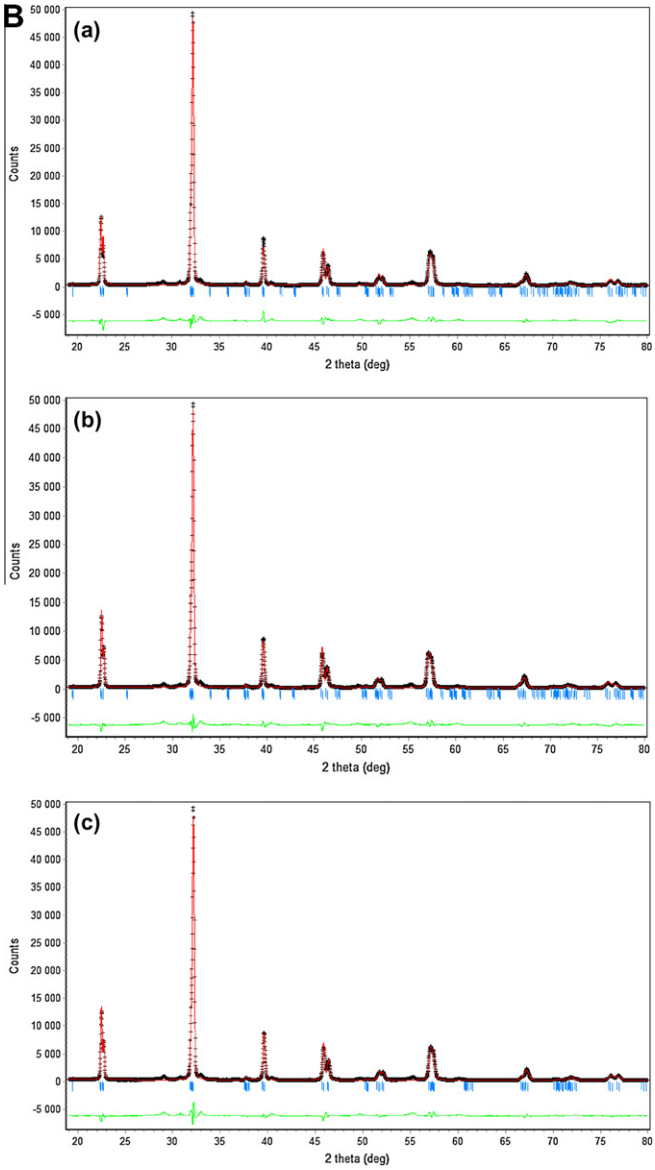

Fig. 2. (*continued*)

Magnetization measurements hysteresis loop were obtained with a Cryogenics VSM magnetometer, up to 10 T.

M(*T*) measurements were performed in a Oxford Instruments VSM, equipped with a furnace, and the measurements were made under a magnetic field of 0.1 T.

3. Results and discussion

3.1. Morphology and crystal structure

The sintering temperature of the $Bi_{1-x}La_xFeO_3$ series increases with lanthanum content at 820–950 °C [12,22,23,27]. The typical morphologies of $Bi_{0.7}La_{0.3}FeO_3$ samples, observed by scanning electron microscopy, are presented in Fig. 1. No significant changes are detected as a function of the preparation method, either sol–gel or co-precipitation. Grain size increases with sintering temperature and time from 0.5 μm in the 820 °C/10 min up to 4 μm in the 870 °C/3 h sintered samples. The differences in the microstructures are only due to the sintering temperature and the sintering time effect. As a result, the apparent density also increases from 4.18 g cm^{-3} (820 °C/10 min) up to 6.51 g cm^{-3} (870 °C/3 h).

In undoped BFO, the percentage of secondary phases increases under higher sintering temperatures [25]. However, no apparent differences were observed in the X-ray diffraction patterns for $Bi_{0.7}La_{0.3}FeO_3$ samples sintered at the temperature range of 830–870 °C using a 3 h thermal treatment, as shown in Fig. 2(A). In addition, no visible differences were observed in the X-ray patterns of the samples prepared by the sol–gel combustion or the co-precipitation methods. This result clearly indicates that La^{3+} doping promotes the stabilization of the perovskite phase. After applying Rietveld refinement (Rietica) to the XRD patterns with the structures P$n2_1a$, P*nma* and I*mma* (Fig. 2(B)), we obtained similar reliability factors, presented in Table 1. The obtained structure parameters are also listed in Table 1. In the case of C*222* group, the R_{wp} obtained was much higher (nearly 16%). Detailed analysis of the refinements (inset of Fig. 2(A)) shows small peaks (signalized with a "∗") that cannot be indexed with any of the proposed structures. These regions were excluded during the simulation to allow the convergence of the refinement (lower *R*-factors). Some authors associate these small peaks to secondary phases [34], however, they systematically appear under different sintering temperatures and different synthesis methods, either in sol–gel combustion or in co-precipitation, so a more defined explanation must be found. In a recent article, Rusakov et al. [16] found peaks at nearly the same *d*-spaces in the synchrotron XRD of $Bi_{0.75}La_{0.25}FeO_3$. The structure was solved by Rietveld refinement using Jana2006 software [31], proposing the I*mma*(*00γ*)*s00* superspace group with an incommensurable modulation vector of $q = 0.4855(4)c^*$ which is caused by a displacement of Bi and O_1 ions along the *a* axis toward each other and by the displacement of the O_2 ion within the *ac* plane [16]. Using Jana2006 and starting with cell parameters obtained in Rietica refinement, we performed the refinement of our XRD data in LeBail pattern match mode. The program had to start from the general P*1*(*αβγ*) and only after we restricted the non centrosymmetric P$n2_1a$(*00γ*)*s00* and the centrosymmetric I*mma*(*00γ*)*s00* superspace groups. The obtained results are listed in Table 2. For all the structures we obtained a q_3 value of around 0.46, which is in accordance with the prediction of Rusakov et al. that the q_3 value decreases as

Table 1
Refined structural parameters for $Bi_{0.7}La_{0.3}FeO_3$ samples (820 °C/10 min) and the compared results with C*222*, I*mma*, P*nma* and P$n2_1a$.

Lattice parameters (Å)	Atomic coordinates				*R* factors (%)	
		x	*y*	*z*		
C*222*	Bi/La	0	0	0	R_p	11.03
a = 5.586(2)	Fe	0.5	0	0.5	R_{wp}	15.97
b = 5.612(2)	O_1	0	0.5	0	χ^2	23.70
c = 3.919(1)	O_2	0	0.224(2)	0.5		
V = 122.89 Å^3						
I*mma*	Bi/La	0.0360(2)	0.2500	0.991(1)	R_p	6.75
a = 5.606(1)	Fe	0	0	0.5000	R_{wp}	8.73
b = 7.831(1)	O_1	0.448(2)	0.2500	0.0857(2)	χ^2	7.32
c = 5.586(1)	O_2	0.2500	0.466(3)	0.2500		
V = 245.27 Å^3						
P*nma*	Bi/La	−0.004(2)	0.2500	0.988(1)	R_p	8.05
a = 5.611(1)	Fe	0	0	0.5000	R_{wp}	11.12
b = 7.837(2)	O_1	0.463(3)	0.2500	0.0101(1)	χ^2	11.43
c = 5.587(2)	O_2	0.2500	0.490(1)	0.2500		
V = 245.75 Å^3						
P$n2_1a$	Bi/La	0	0.258(2)	0.993(1)	R_p	7.21
a = 5.604(2)	Fe	0	0	0.5000	R_{wp}	9.66
b = 7.828(1)	O_1	0.594(3)	0.217(5)	−0.005(3)	χ^2	9.34
c = 5.582(2)	O_2	0.222(1)	0.473(1)	0.210(2)		
V = 244.93 Å^3	O_3	0.760(2)	0.539(1)	0.754(1)		

Table 2
Results of refinement with Jana2006 for $Bi_{0.7}La_{0.3}FeO_3$ sample (870 °C/3 h) and P1($\alpha\beta\gamma$), P$n2_1a(00\gamma)s00$, and I$mma(00\gamma)s00$ superspace groups.

Superspace group	Cell and incommensurate vector parameters			*R* factors (%)
P1($\alpha\beta\gamma$)	a = 5.613(2) Å α = 90.03(2)° q_1 = 0.0076(1)	b = 7.814(1) Å β = 90.05(2)° q_2 = 0.0136(1)	c = 5.588(2) Å γ = 89.96(1)° q_3 = 0.457(2)	R_p = 3.79 R_{wp} = 5.55
P$n2_1a(00\gamma)s00$	a = 5.623(2) Å	b = 7.826(2) Å	c = 5.597(1) Å q_3 = 0.465(2)	R_p = 5.65 R_{wp} = 8.57
I$mma(00\gamma)s00$	a = 5.609(2) Å	b = 7.830(1) Å	c = 5.585(1) Å q_3 = 0.457(1)	R_p = 6.05 R_{wp} = 9.14

the La content increases (see inset plot in Fig. 3 (a). The obtained refinement factors are similar in the P$n2_1a(00\gamma)s00$ and I$mma(00\gamma)s00$, and lower in the P1($\alpha\beta\gamma$). Nevertheless, the most important aspect of these refinements is that the small peaks are indeed satellite peaks originated by the incommensurated modulated structure and that they are not peaks from secondary phases.

Besides the *R* factors in the analysis of the refinement results, visual comparison between simulated pattern and experimental

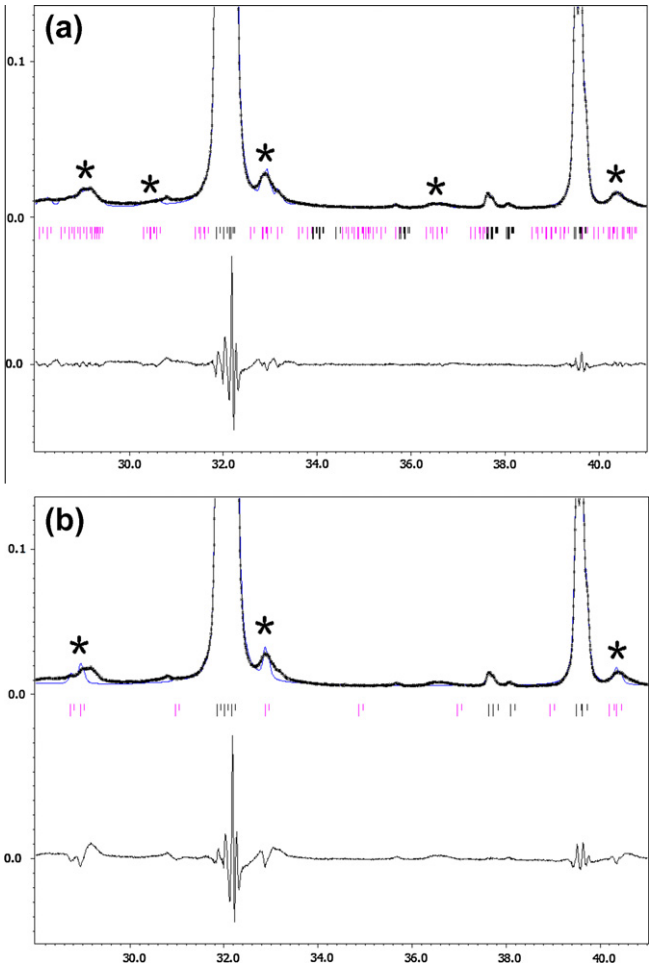

Fig. 3. Refinement of the XRD pattern of the $Bi_{0.7}La_{0.3}FeO_3$ sample with Jana2006 and LeBail pattern match mode. The predicted positions of the small peaks of the incommensurated modulated structure are marked. (a) Magnification of the refinement with P1($\alpha\beta\gamma$) superspace group. (b) Magnification of the refinement with I$mma(00\gamma)s00$ superspace group. (c) Magnification of the refinement with P$n2_1a(00\gamma)s00$ superspace group. (d) Full XRD spectrum refined with I$mma(00\gamma)s00$ superspace group and data from Table 3; insert the value of the modulation vector γ as a function of x in $Bi_{1-x}La_xFeO_3$.

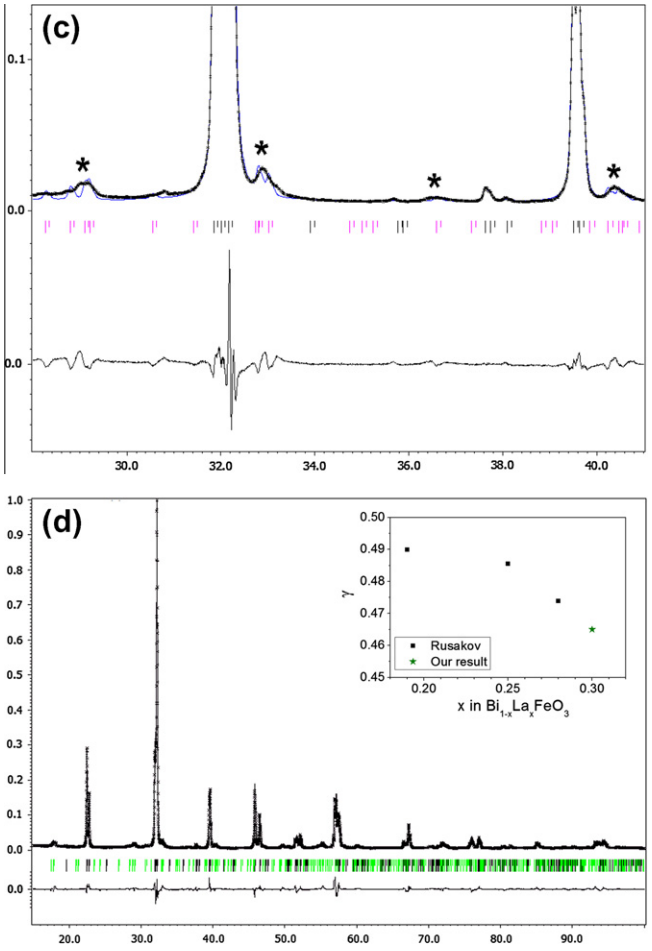

Fig. 3. (*continued*)

data is very important. In Fig. 3(b–d) magnifications of the refinement graphs are showed for the three structures. In Fig. 3(b) we see that the satellite peaks of the I$mma(00\gamma)s00$ structure do not fit exactly the experimental pattern, specifically the peaks at $2\theta \approx 29°$ and 33°. In that way, the P$n2_1a(00\gamma)s00$ structure is more accurate due to the fact that it predicts more than one satellite peak to that position. Moreover, the P$n2_1a(00\gamma)s00$ structure predicts a peak at $2\theta \approx 25°$ (see Fig. 3(d) which is not predicted in the I$mma(00\gamma)s00$ structure. Looking carefully at the experimental pattern we can confirm that a very small peak is present at $2\theta \approx 25°$. These differences justify the lower *R*-factors of that structure. The calculated values for P1($\alpha\beta\gamma$) structure, Table 2, indicate a small deviation from an orthorhombic symmetry (α, β and γ are close to 90°). Moreover, the values of q_1 and q_2 are quite small, resulting in very long modulation periods, which is not likely to occur.

The full refinement with atomic positions was performed with the non centrosymmetric P$n2_1a(00\gamma)s00$ super structure. This structure was selected taking into account these previous refinement results, but also the ferroelectric and piezoelectric behavior. Cell and incommensurated modulated vector parameters, atomic position, distances and angles are presented in Table 3. The distances and angles are average because of the modulated structure.

Raman spectroscopy was employed to further investigate the structural changes induced by the La-doping. The unpolarized Raman spectra of $Bi_{1-x}La_xFeO_3$ (x = 0 and x = 0.30), recorded at room temperature, are presented in Fig. 4. According to group theory, pure $BiFeO_3$ with rhombohedral *R3c* structure has 12 Raman active

Table 3
Final results of refinement of atomic positions, distances and angles with Jana2006 for $Bi_{0.7}La_{0.3}FeO_3$ sample (870 °C/3 h) and $Pn2_1a(00\gamma)s00$ superspace group.

Superspace group	Cell and incommensurate vector parameters	Atomic positions	*R* factors (%)
$Pn2_1a(00\gamma)s00$	a = 5.6177(1) Å b = 7.8174(2) Å c = 5.5926(1) Å q_3 = 0.465(1)	Bi/La (0, 0.25, 0.9915(1) Fe (0, 0, 0.5) O_1 (0.5743(1), 0.25, 0.0786(2)) O_2 (0.25, 0.5266(1), 0.2490(2) O_3 (0.2053(1), 0.5570(2), 0.8145(1))	R_p = 9.65 R_{wp} = 13.29

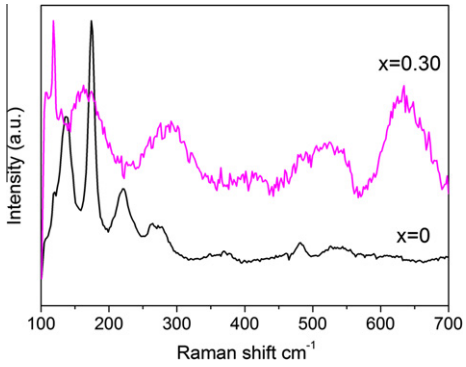

Fig. 4. Raman spectra of $Bi_{1-x}La_xFeO_3$ samples (820 °C/10 min). The spectra are normalized to the highest intense peak.

modes: $4A_1$ and 8E [35]. The Raman spectrum of $BiFeO_3$ was well fitted with 12 bands, which peak positions are indicated in Table 4. The most intense peaks are located at 137, 174 e 221 cm^{-1}, in agreement with the reported values [36,37]. The low frequency modes have been assigned to relative motion of A-site cations; in particular the A_1 modes are related with Bi–O band. Raman modes of higher frequency are related to the stretching and the bending of Fe–O [38]. The peak positions for $BiFeO_3$ are in agreement with published results, taking into account that different preparation methods slightly changes the wave number of the oxygen vibration modes [39,40]. Raman measurements in La-doped samples indicate that peaks at 260 and 221 cm^{-1} became weaker and cannot be detected for $x > 0.15$, and the peak around 610 cm^{-1} shifts to higher frequencies as the La content increases [41].

The Raman spectrum of the $x = 0.30$ sample exhibits very low intensity, compared with pure $BiFeO_3$, and rather broad bands that could be fitted considering 8 bands (Table 3). Some modes appear to merge into several broad bands, which can be due to the increase of structural disorder caused by the raise of lanthanum content [42,43]. The number of bands predicted for I*mma* structure is 9 Raman modes, for $Pn2_1a$ it is 12 Raman modes. The obtained results are an argument against the P*nma* structure (18 Raman modes) unless a large number of modes are merged.

3.2. Polar and magnetic properties

In literature there are still a lot of controversy about the ferroelectric origin in the $Bi_{1-x}La_xFeO_3$ series ($x > 0.10$), which could be related to the co-existence of *R3c* phase together with an orthorhombic centrosymmetric phase [18] or originated in the incommensurable structure [16]. In order to investigate this issue we have performed several ferroelectric measurements in different samples with $x = 0.30$ composition.

In the electric or dielectric measurements, the main problem, which arose during conventional ferroelectric measurements of this system, is their high leakage current. Fig. 5(a) shows the leakage current density dependence with the electric field for samples prepared at 820 °C for 10 min. It is observed that the leakage current density of $Bi_{0.70}La_{0.30}FeO_3$ samples is rather low, near 9.2×10^{-7} A cm^{-2} at 1 kV cm^{-1}, and about four orders of magnitude lower than the undoped BFO ceramic sample (not shown here). Moreover, at low electric field (<0.2 kV/cm) there is a rapid increase of the leakage current. At higher fields, the leakage current still exhibits an increase with the applied field compatible with ohmic behavior (see insert plot in Fig. 5(a)). As we have stated above, the substitution of lanthanum by bismuth yields the stabilization of a monophasic perovskite structure. The interpretation of this issue could be attributed to the higher strength of the La–O bond (799 ± 13 kJ mol^{-1}) relative to the Bi–O one (343 ± 6 kJ mol^{-1}) [44]. This difference could also explain the lowering of the oxygen vacancies concentration.

Fig. 5(b) shows the frequency dependence of dielectric constant and losses at room temperature. The dielectric constant at 100 kHz for $Bi_{0.7}La_{0.3}FeO_3$ is 143. This value is comparable to typical values of perovskite type materials ($PbTiO_3$) in which the polarization comes from the A site [1]. The dielectric constant obtained in the sample doped with 30% of lanthanum is higher than the one in the undoped sample ($\varepsilon' = 93$), which is apparently due to the reduction of oxygen vacancies. The dielectric constant slightly decreases when the frequency is increased.

For the undoped $BiFeO_3$ system higher dielectric losses are observed (0.6) which could be associated with structural defects, such as secondary phases, grain boundary conduction and oxygen vacancies. The lanthanum doped composition presented low dielectric losses (0.01) in agreement with the absence of secondary phases and with the reduction of oxygen vacancies, which is in accordance with the results of leakage current density.

The low leakage current observed in the $Bi_{0.7}La_{0.3}FeO_3$ samples show that hysteresis cycles might be experimentally observed if a spontaneous polarization is present [45]. In order to prevent any dynamical response from masking the actual domain reversal, we have chosen to perform the measurements of the $P(E)$ at low operating frequencies of 1.3 Hz. Fig. 5(c) presents room temperature ferroelectric hysteresis loop of a $Bi_{0.7}La_{0.3}FeO_3$ ceramic sample treated at 840 °C/10 min. A typical $P(E)$ loop was obtained meaning that the electric leakage current was greatly reduced with lanthanum substitution. The remnant polarization determined from hysteresis loop is ~0.025 μC cm^{-2} and the coercive electric field is ~1 kV/cm. Zhang [46] reported a very weak polarization of 0.2 μC/cm^2 for ceramic bismuth ferrite and as for other ion doped ceramic samples, Puli [47] observed also a weak polarization of 0.025 μC/cm^2 on his samples. The obtained $P(E)$ loops depend on

Table 4
Dependence of the Raman shift of some bands for $Bi_{1-x}La_xFeO_3$.

Wavenumber (cm^{-1})													
x	E	A1	A1	A1	E		E	E	E	E	E	E	
0	119	137	174	221	261	275	350	371	–	481	538	609	696
0.30	117	155	181	–	–	294	–	410	–	497	534	642	–

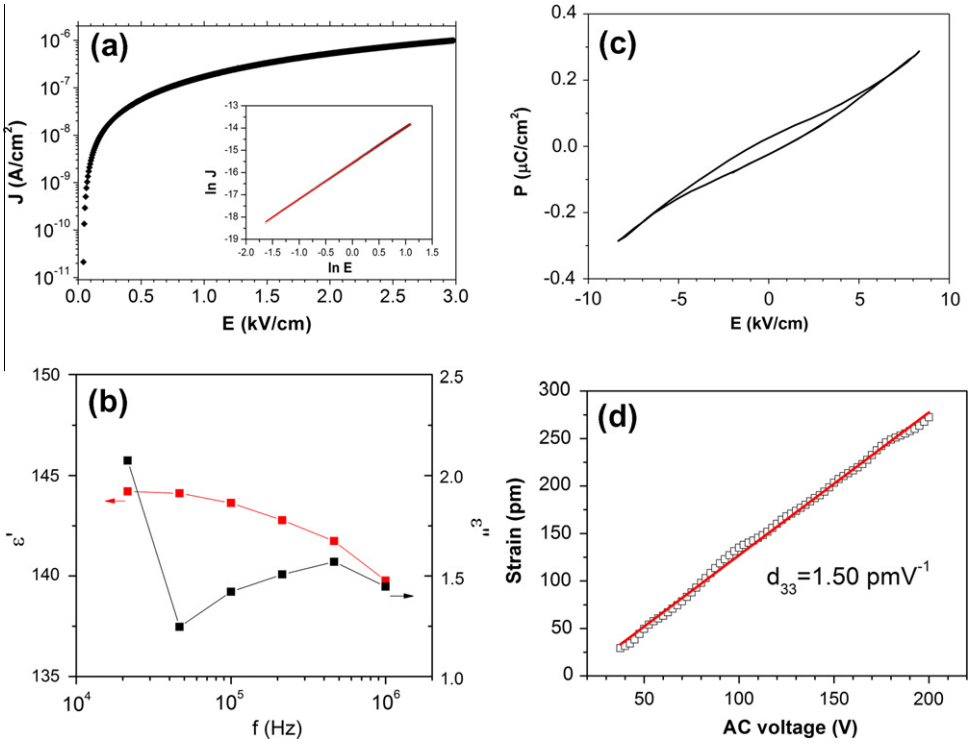

Fig. 5. Electric properties at room temperature for $Bi_{0.7}La_{0.3}FeO_3$ ceramics. (a) Leakage current; the insert is a fit to ohmic behavior; (b) dielectric constant and dielectric losses; (c) ferroelectric polarization cycle at 1.3 Hz sample sintered at 840 °C/10 min; (d) piezoelectric response. Samples sintered at 820 °C/10 min (a) and (b)) or at 840 °C/10 min (c) and (d)).

the sintering temperature and on the aging of the samples, as predicted by Troyanchuk [18], but not on the processing conditions, sol–gel or co-precipitation. The full study of this behavior will be the main topic of a future publication. The existence of a remnant polarization is in favor for a non-centrosymmetric $P n 2_1 a(00\gamma)s00$ structure.

In this work, we have obtained for the d_{33} piezoelectric coefficient of $Bi_{0.7}La_{0.3}FeO_3$ a value of 1.50 pm V^{-1} (Fig. 5(d)), which had never been reported before. According to Jiang et al. the maximum value is obtained around $x = 0.05$ and decreases for higher La content [17]. Catalan et al. mention that the low piezoelectric constant of proper ferroelectrics/improper ferroelastics with a centrosymmetric paraphase is related to the low dielectric constant and the low polarization [1]. Other perovskite ferroelectrics, like $BaTiO_3$, where the polarization comes from the B site, can present much higher values, within the 100–1000 pm V^{-1} range.

Fig. 6(a) shows a magnetization loop of the $Bi_{0.7}La_{0.3}FeO_3$ sample, clearly indicating the presence of a weak ferromagnetic behavior at room temperature. The remnant magnetization is 0.30 emu g^{-1} and the coercive field is 0.71 T. The enhancement of magnetic properties, when compared with less doped compositions (see inset plot in Fig. 6(a)), is associated with the structural change from rhombohedric to orthorhombic that results in a modification on the modulated spiral spin [48]. It was also measured the magnetization as a function of the temperature. In fig. 6(b) we present the result for the $x = 0.30$ sample. The temperature dependence of the magnetization is common for a ferromagnetic material, see Eq. (2) [49]:

$$\frac{M(T)}{M(0)} = B\left(1 - \frac{T}{T_c}\right)^{\beta} \quad (2)$$

Fitting the Eq. (2) to the experimental data at $T < T_c$, where $M(T)$ is the zero field magnetization at T temperature, B is a coefficient that vary slightly from system to system and is generally of the unity order, and β is the critical exponent, we could obtain a critical exponent of $\beta = 0.353 \pm 0.001$, $T_c = 671 \pm 1$ K and $B = 1.38 \pm 0.01$.

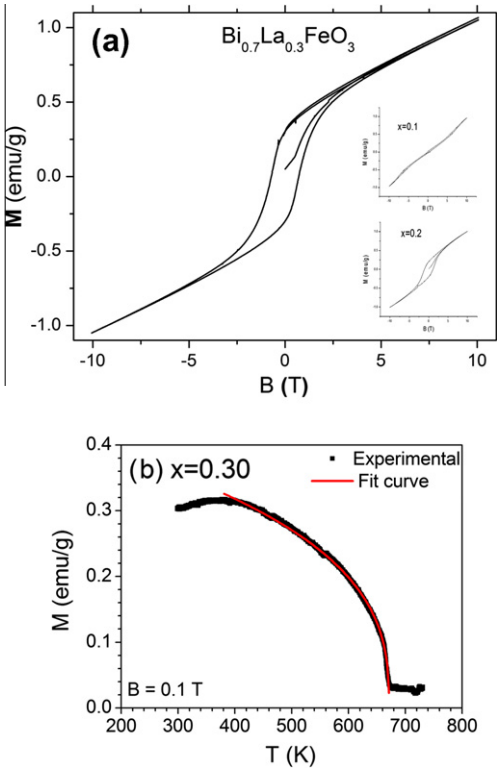

Fig. 6. (a) Magnetization as function of the magnetic field at room temperature. (b) $M(T)$ measurement and fitting results with Eq. (2).

Critical exponent near 1/3 or slightly higher is in good agreement with the one expected from 3-dimensional Heisenberg exchange models [49]. Lower values of the critical exponent could mean that the magnetic behavior is still affected by some spiral spin arrangement. The obtained value indicates that the spiral spin arrangement is completely destroyed in the $x = 0.30$ composition.

4. Conclusions

Ceramic $Bi_{0.7}La_{0.3}FeO_3$ samples were successfully synthesized by sol–gel combustion and co-precipitation methods. Rietveld refinements of the XRD data detected small satellite peaks that were successfully indexed by an incommensurated modulated structure model. This modulation is caused by a displacement of Bi and O_1 ions along the *a* axis toward each other and by the displacement of the O_2 ion within the *ac* plane. The results of the XRD refinements, the ferroelectric and piezoelectric behavior are in favor for a non-centrosymmetric $Pn2_1a(00\gamma)s00$ structure, with $a = 5.623(6)$ Å, $b = 7.826(5)$ Å, $c = 5.597(0)$ Å, $q_3 = 0.465(5)$. The samples presented a low leakage current of 9.2×10^{-7} A cm^{-2} at 1 kV cm^{-1} fitted by an ohmic model. Dielectric constant (143 at 100 kHz), dielectric losses (<0.02) and piezoelectric coefficient (1.5 pm V^{-1}) are low. Weak ferromagnetic behavior was also observed at room temperature ($M_r = 0.30$ emu g^{-1}).

Acknowledgments

This work was supported by the Fundação para a Ciência e Tecnologia (FCT) of Portugal through projects PTDC/CTM/99415/2008, PTDC/FIS/105416/2008, CERN/FP/109357/2009, CERN/FP/116320/2010 and CQVR/PEst-C/QUI/UI0616/2011. T. T. Carvalho also acknowledges the FCT for the PhD grant (SFRH/BD/41331/2007).

References

[1] G. Catalan, J.F. Scott, Adv. Mater. 21 (2009) 2463.
[2] Y.H. Chu, L.W. Martin, et al., Nat. Mater. 7 (2008) 478.
[3] K. Takahashi, N. Kida, et al., Phys. Rev. Lett. 96 (2006) 117402.
[4] S. Li, Y.-H. Lin, et al., J. Phys. Chem. C 114 (2010) 2903.
[5] J. Silva, A. Reyes, H. Esparza, H. Camacho, L. Fuentes, Integr. Ferroelectr. 126 (2011) 47.
[6] J. Wang, J.B. Neaton, et al., Science 299 (2003) 1719.
[7] J. Wu, G. Kang, et al., Appl. Phys. Lett. 95 (2009) 192901.
[8] Y. Li, Y. Yang, et al., Appl. Phys. Lett. 101 (2012) 022905.
[9] I.O. Troyanchuk, D.V. Karpinsky, et al., J. Am. Ceram. Soc. 94 (2011) 4502.
[10] P. Kharel, S. Talebi, et al., J. Phys.: Condens. Matter. 21 (2009) 036001.
[11] Y. Yao, W. Liu, et al., Int. J. Appl. Ceram. Technol. 8 (2011) 1246.
[12] Q.-H. Jiang, C.-W. Nan, Z.-J. Shen, J. Am. Ceram. Soc. 89 (2006) 2123.
[13] A.Z. Simões, F.G. Garcia, C.S. Riccardi, Mater. Chem. Phys. 116 (2009) 305.
[14] R. Rai, S.K. Mishra, N.K. Singh, S. Sharma, A.L. Kholkin, Curr. Appl. Phys. 11 (2011) 508.
[15] Z.V. Gabbasova, M.D. Kuz'min, A.K. Zvezdin, I.S. Dubenko, V.A. Murashov, D.N. Rakov, I.B. Krynetsky, Phys. Lett. A 158 (1991) 491.
[16] D.A. Rusakov, A.M. Abakumov, K. Yamaura, A.A. Belik, G.V. Tendeloo, E.T. Muromachi, Chem. Mater. 23 (2011) 285.
[17] I.O. Troyanchuk, D.V. Karpnisky, M.V. Bushinsky, O.S. Mantytskaya, N.V. Tereshko, V.N. Shut, J. Am. Ceram. Soc. 94 (2011) 4502.
[18] I.O. Troyanchuk, M.V. Bushinsky, D.V. Karpinsky, O.S. Mantytskaya, V.V. Fedotova, O.I. Proknenko, Phys. Status Solidi B 246 (2009) 1901.
[19] T.-J. Park, G.C. Papaefthymiou, A.J. Viescas, A.R. Moodenbaugh, S.S. Wong, Nano Lett. 7 (2007) 766.
[20] J. Wang, J.B. Neaton, H. Zheng, V. Nagarajan, S.B. Ogale, B. Liu, D. Viehland, V. Vaithyanathan, D.G. Schlom, U.V. Waghmare, N.A. Spaldin, K.M. Rabe, M. Wuttig, R. Ramesh, Science 299 (2003) 1719.
[21] X. Wang, Y. Lin, X. Ding, J. Jiang, J. Alloys Comp. 509 (2011) 6585.
[22] Y.-H. Lin, Q. Jiang, Y. Wang, C.-W. Nan, Appl. Phys. Lett. 90 (2007) 172507.
[23] J.R. Sahu, C.N.R. Rao, Solid State Sci. 9 (2007) 950.
[24] Z.X. Cheng, A.H. Li, X.L. Wang, S.X. Dou, K. Ozawa, H. Kimura, S.J. Zhang, T.R. Shrout, J. Appl. Phys. 103 (2008) 7E507.
[25] T.T. Carvalho, P.B. Tavares, Mater. Lett. 62 (2008) 3984.
[26] H. Ke, W. Wang, Y. Wang, J. Xu, D. Jia, Z. Lu, Y. Zhou, J. Alloys Comp. 509 (2011) 2192.
[27] S.T. Zhang, M.H. Lu, D. Wu, Y.F. Chen, N.B. Ming, Appl. Phys. Lett. 87 (2005) 262907.
[28] Y.P. Wang, L. Zhou, M.F. Zhang, X.Y. Chen, J.M. Liu, Z.G. Liu, Appl. Phys. Lett. 84 (2004) 1731.
[29] W. Kraus, G. Nolze, PowderCell for Windows, version 2.3. Available from: <http://www.ccp14.ac.uk/ccp/web-mirrors/powdcell/a_v/v_1/powder/e_cell.html>, 2011 (accessed September, 2011).
[30] B. Hunter, International Union of Crystallography Commission on Powder Diffraction Newsletter No. 20. Available at: <http://www.rietica.org>, 1998 (accessed September, 2011).
[31] Vaclav Petrick, Michal Dusek, Lukas Palatinus, Available from: <http://www-xray.fzu.cz/jana/jana.html> (accessed November, 2011).
[32] C.B. Sawyer, C.H. Tower, Phys. Rev. 35 (1930) 269.
[33] J.R. Fernandes, F.A. De Sá, J.L. Santos, E. Joanni, Rev. Sci. Instrum. 73 (2002) 2073.
[34] I.O. Troyanchuk, D.V. Karpinsky, M.V. Bushinsky, O.S. Mantyskaya, N.V. Tereshko, V.N. Shut, J. Am. Ceram. Soc. 94 (2011) 4502.
[35] E. Kroumova, M.I. Aroyo, J.M. Perez Mato, A. Kirov, C. Capillas, S. Ivantchev, H. Wondratschek, Phase Transitions 76 (1–2) (2003) 155.
[36] G.L. Yuan, S.W. Or, H.L.W. Chan, J. Phys. D: Appl. Phys. 40 (2007) 1196.
[37] M. Cazayous, J. Gallais, A. Sacuto, R.D. Sousa, D. Lebeugle, D. Colson, Phys. Rev. Lett. 101 (2008) 037601.
[38] P. Kharel, S. Talebi, B. Ramachandran, A. Dixit, V.M. Naik, M.B. Sahara, C. Sudakar, R. Naik, M.S.R. Rao, G. Lawes, J. Phys.: Condens. Matter. 21 (2009) 036001.
[39] S.-T. Zhang, L.-H. Pang, Y. Zhang, M.-H. Lu, Y.-F. Chen, J. Appl. Phys. 100 (2006) 114108.
[40] D. Kothari, V.R. Reddy, V.G. Sathe, A. Goupta, A. Banerjee, A.M. Awasthi, J. Magn. Magn. Mater. 320 (2008) 548.
[41] Y. Yang, K. Yu-Long, Z. Ke, Z. Li-Yan, M. Shu-Yuan, L. Jie, J. Yi-Jian, Chin. Phys. B 19 (2010) 037802.
[42] P.S. Dobal, R.S. Katiyar, J. Raman Spectrosc. 33 (2002) 405.
[43] G. Kartopu, A. Lahmar, S. Habouti, C.L. Solterbeck, B. Eloudi, M. Es-Souni, Appl. Phys. Lett. 92 (2008) 151910.
[44] John A. Dean, Lange's Handbook of Chemistry, 15th ed., McGraw Hill, New York, 1999.
[45] Z.X. Cheng, A.H. Li, X.L. Wang, S.X. Dou, K. Ozawa, H. Kimura, S.J. Zhang, T.R. Shrout, J. Appl. Phys. 103 (2008) 07E507.
[46] X. Zhang, Y. Sui, X. Wang, Y. Wang, Z. Wang, J. Alloys Comp. 507 (2010) 157.
[47] V.S. Puli, A. Kumar, N. Panwar, R.S. Katiyar, J. Alloys Comp. 509 (2011) 8223.
[48] V.S. Pokatilov, V.V. Pokatilov, A.S. Sigov, Phys. Solid State 51 (2009) 552.
[49] H.E. Stanley, Introduction to Phase Transitions and Critical Phenomena, Oxford University Press, Oxford, 1987.